ISSN 0915-633X

NATIONAL INSTITUTE FOR FUSION SCIENCE

R & D of Transmission Lines for ECH System

K. Ohkubo, M. Hosokawa, S. Kubo, M. Sato,
Y. Takita and T. Kuroda

(Received – Jan. 27, 1993)

NIFS-210 Feb. 1993

RESEARCH REPORT
NIFS Series

NAGOYA, JAPAN

R&D of Transmission Lines for ECH System

K. Ohkubo, M. Hosokawa, S. Kubo, M. Sato,
Y. Takita and T. Kuroda
National Institute for Fusion Science, Furo-cho,
Chikusa-ku, Nagoya, 464-01, Japan

Received

ABSTRACT

The performance of oversized transmission elements for millimeter waves is measured and compared with the calculation which is based on the superposition of plane wave (SPW) and on Fresnel approximation in the Huygens-Kirchhoff integral. Mode-conversion in the split waveguide is discussed from the viewpoint of on- and off-axes and 90-degrees elbow bend on phase correction is examined by using the SPW method. The design and experiment on the whispering gallery mode generator are described. A preliminary analysis of the rectangular waveguide with two corrugated plates and two plane walls is also carried out to obtain the Gaussian beam with a waist size of x-axis different from that of y-axis.

Keywords:radiation pattern, FFT, coupling of split waveguide, phase-correction bend, rectangular waveguide, rotating-whispering-gallery mode generator

§ 1. Introduction

In the recent device for fusion reseach, high-power millimeter waves have been increasingly used in the electron cyclotron heating and current drive of toroidal plasmas. At present, power level is being increased up to MW-class. As mode of transmission for millimeter waves, hybrid mode such as HE-mode is used recently due to their low loss and linear-like polarization. In this paper we describe a evaluation-method for performance of transmission elements and designs for some transmission elements with HE_{11} mode.

§ 2. Radation Pattern and Detection

The diffraction in electromagnetic wave and light has been calculated traditionally by using the Huygens-Kirchhoff principle. More recently the radiation pattern derivered from the superposition of plane wave (SPW) in different directions by using the only transverse electric fields (E_x and E_y) and Maxwell equation [1]. We modify the SPW method in order to draw radiation patterns for near field by both transverse electric and magnetic fields (H_x and H_y). For far field, we apply Fresnel approximation in the Huygens-Kirchhoff integral. Here, FFT and inverse FFT are adopted for the advantage of increase in the calculation speed. When wave whose amplitude is normalized by the orthnormal relation propagates along z-direction, EM-field at any z can be written in terms of their spectrum functions $\vec{S}_t\ (k_x,\ k_y)$ and $\vec{Q}_t\ (k_x,\ k_y)$ which are calculated from the Fourier transformation of the transverse EM-field $\vec{E}_{twg}\ (x_1,\ y_1)$ and $\vec{H}_{twg}\ (x_1,\ y_1)$ at the aperture $(z_1 = 0)$;

$$\vec{S}_t(k_x, k_y) = \int\int \vec{E}_{twg}(x_1, y_1)\exp[i(k_x x_1 + k_y y_1)]dx_1 dy_1 \tag{1}$$

$$\vec{Q}_t(k_x, k_y) = \int\int \vec{H}_{twg}(x_1, y_1)\exp[i(k_x x_1 + k_y y_1)]dx_1 dy_1. \tag{2}$$

The longitudinal spectrum functions for E_z and H_z are determined by $\vec{k}\cdot\vec{S} = 0$ and $\vec{k}\cdot\vec{Q} = 0$. Radation pattern is given by

$$\vec{E}(x, y, z) = \frac{1}{4\pi^2}\int\int \frac{k_z\vec{S}_t - (k_t\cdot\vec{S}_t)\vec{i}_z}{k_z}\exp[-i(k_x x + k_y y + k_z z)]dk_x dk_y \tag{3}$$

$$\vec{H}(x, y, z) = \frac{1}{4\pi^2}\int\int \frac{k_z\vec{Q}_t - (k_t\cdot\vec{Q}_t)\vec{i}_z}{k_z}\exp[-i(k_x x + k_y y + k_z z)]dk_x dk_y. \tag{4}$$

Here, k_z depends on k_x and k_y

$$k_z = \sqrt{k_0^2 - k_x^2 - k_y^2} \quad \text{when} \quad k_0^2 \geq k_x^2 + k_y^2 \tag{5}$$

(6) $$k_z = -i\sqrt{k_0^2 - k_x^2 - k_y^2} \quad \text{when} \quad k_0^2 < k_x^2 + k_y^2.$$

The fields of $\vec{E}_{twg}$ and $\vec{H}_{twg}$ at the aperture of the waveguide are calculated by incident fields to the aperture $\vec{E}_{ti}$ (x_1, y_1) and $\vec{H}_{ti}$ (x_1, y_1) with reflection coefficient Γ,

(7) $$\vec{E}_{twg} = (1 + \Gamma)\vec{E}_{ti}$$

(8) $$\vec{H}_{twg} = (1 - \Gamma)\vec{H}_{ti}$$

(9) $$\Gamma = (1 - s)/(1 + s)$$

(10) $$s = \vec{H}_{ti}/[(\vec{i}_z \times \vec{E}_{ti})Z_0]$$

where, Z_0 is the intrinsic impedance in vacuum and $s = \lambda/\lambda_g$ for TE mode and $s = \lambda_g/\lambda$ for TM mode. For HE and EH modes, s must be directly evaluated by the result from transverse fields in the corrugated waveguide [2]. Except for the high higer-mode in the oversized waveguide, s is nearly equal to unity.

The opening surface A on $x_1 - y_1$ plane with the size of $L \times L$ consists of the aperture and the exterior surface of the aperture. The transverse electric field over the exterior surface is zero. Here, $\vec{H}_t$ is assumed to be zero on the waveguide surface. This is increasingly better approximation as the aperture size increases. In order to perform DFT, the surface A on $x_1 - y_1$ including the aperture is sampled with $M \times M$. In the spectrum plane on $k_x/2\pi - k_y/2\pi$, function $\exp(-ik_z z)$ is also sampled in the same way. It is required that the phase change in this function between neighboring sampling points is less than π. The phase change to any sampling points (m_s, n_s) with $k_x/2\pi = m_s/L$ and $k_y/2\pi = n_s/L$ $(-M/2 < m_s, n_s < M/2)$ is approximately given by $|(2\pi/L) \cdot d(k_z z)/dk_r| \leq \pi$, where, $k_r = \sqrt{k_x^2 + k_y^2}$. This equation can be written as

(11a) $$m_s^2 + n_s^2 \leq \frac{(L/\lambda)^2}{1 + (2z/L)^2} = R_{SPW}^2$$

(11b) $$m_s^2 + n_s^2 \leq (\frac{L^2}{2\lambda z})^2 \quad \text{for large } z$$

where $m_s^2 + n_s^2 \leq (L/\lambda)^2$ corresponding to the propagation in free space is automatically satisfied. Because FFT and inverse FFT are in use of the calculation, it is noted that

the total surface size on $x-y$ plane at any z becomes the same as $L \times L$ on $x_1 - y_1$ plane. The calculated radiation pattern with $M/2 < R_{SPW}$ for certain z is valid over all the opening surface A at x - y plane. Even if $M/2 > R_{PSW}$, the numerical calculation is valid for the region B satisfying eq.(11).

Because the region B becomes small for large z in far field, we put the Fresnel transformation (FT) by approximating the Huygens-Kirchhoff integral to practical use with the aid of FFT in stead of SPW;

$$\vec{E}_t(x,y,z) = \frac{i}{\lambda z}\exp(-\frac{2\pi z i}{\lambda})\exp[-\frac{i\pi}{\lambda z}(x^2+y^2)] \tag{12}$$
$$\times \int\int \vec{E}_{twg}(x_1,y_1)\exp[-\frac{i\pi}{\lambda z}(x_1^2+y_1^2)]$$
$$\times\exp[-\frac{2\pi i}{\lambda z}(x_1 x + y_1 y)]dx_1 dy_1. \quad \text{etc.}$$

Because the sampling width on $x_1 - y_1$ plane is $\lambda z/L$, the total opening size is equal to $M\lambda z/L \times M\lambda z/L$. It should be noted that the sampling width becomes larger when distance z increases. It is necessary that the phase change between neighboring points in $\exp\,[-(i\pi/\lambda z)\cdot(x_1^2+y_1^2)]$ is less than π as discussed before. We obtain

$$m_s^2 + n_s^2 \quad \leq (\lambda z M^2/2L^2)^2 = R_{FT}^2 \tag{13}$$

It should be pointed out that the center of radiation pattern is displaced in the FFT calculation according as z. We obtain the radation pattern whose center is located at $m_s = p_0$ and $n_s = q_0$ by puting back the displacement and considering the aliasing effect. The displacements p and q from $m_s = p_0$ and $n_s = q_0$ along x- and y- axes are written as [3]

$$p = p_0\frac{L^2}{\lambda z M} \quad \text{and} \quad q = q_0\frac{L^2}{\lambda z M} \tag{14}$$

where p_0 and q_0 is the sampling number at the center on the opening surface A. By comparing eq.(11b) with eq.(13), the SPW method should be adopted for $z \leq L^2/\lambda M$. When the radiation is detected by the standard waveguide (for instance WR-10) installed along z-direction, two configurations of waveguide are performed for the purpose of measurement in normal and cross polarizations. From Maxwell equation, we obtain Poynting flux P_{zn} and P_{zc} with $E_x = 0$ and $E_y = 0$ for normal and cross polarizations, respectively.

$$P_{zn} = (1/2)\mathrm{Re}[(k_y|E_y|^2 - k_z E_y E_z^*)/(k_0 Z_0)] \tag{15}$$

$$= (1/2)\mathrm{Re}[(k_x H_x^* H_z - k_z |H_x|^2) Z_0/k_0]$$

(16)
$$P_{zc} = (1/2)\mathrm{Re}[(k_z |E_x|^2 - k_x E_x E_z^*)/(k_0 Z_0)]$$
$$= (1/2)\mathrm{Re}[(k_y H_y^* H_z - k_z |H_y|^2) Z_0/k_0]$$

For TE mode, P_{zn} and P_{zc} are proportional to $|E_y|^2$ and $|E_x|^2$, respectively. With respect to TM mode, those are proportional to $|H_y|^2$ and $|H_x|^2$. For hybrid modes (HE and EH modes) having both small E_z and H_z fields, P_{zn} (P_{zc}) is approximately proportional to $|E_y|^2$ or $|H_x|^2$ ($|E_x|^2$ or $|H_y|^2$).

We measure the radiation patterns from the HE_{11}-mode convertor and compare with the calculation. Figure 1 shows the experimental and calculated results of radiation pattern with normal and cross polarized configurations for the corrugated waveguide with 16.25 mm in diameter as a parameter of z. The calculation is carried out with pure HE_{11} mode. Normal pattern at $z = 2$ and 30 cm, however, suggests little mixing with of EH_{12} mode. Cross polarized pattern is asymmetric because of the existence of EH_{12} mode. The experimental P_{cmax}/P_{nmax} which is the ratio of the maximum in P_{zc} to that in P_{zn} is -28 ± 2 db and the calculated value is -45.8 db for various z. The difference is caused by sprious EH_{12} mode of 0.16 %.

When the corrugated waveguide with 16.25 mm in diameter is connected to the tapered corrugated-waveguide to 88.9 mm in diameter measured radation patterns are in good agreement with HE_{11} mode including EH_{12} mode. Here, experimental P_{cmax}/P_{nmax} is equal to -28 db. It is shown that no suprious mode increases when the tapered waveguide is connected.

§ 3. Coupling Analysis of Split Waveguide

Split waveguide system consists of the lauching waveguide and the receiving one with the gap distance z. The system is ideal for the DC break in the transmission line and for radial extraction of electron beam from the gap in the gyrotron. We restrict our attension to the mode purity and its content in the split waveguide with on- and off-axes receiving waveguide. As discussed in § 1, an amplitude of reflected wave Γ is nearly equal to zero for low higer-mode in the oversized waveguide. The analysis is carried out by neglecting a reflected wave at the waveguide aperture. In the $x-y$ plane at z where the receiving waveguide is located, the EM-field $\vec{E}\ (x, y, z)$ and $\vec{H}\ (x, y, z)$ radiated from the waveguide aperture is written by

(17)
$$\vec{E} = \sum_m A_m(z)\vec{E}_m + \vec{E}_{out}$$

(18) $$\vec{H} = \sum_m A_m(z)\vec{H}_m + \vec{H}_{out}$$

where A_m is complex amplitude of electric and magnetic fields for m mode in the receiving waveguide, and $\vec{E}_{out}$ ($\vec{H}_{out}$) is the EM-fields outside of the receiving waveguide. In the receiving waveguide, the orthogonality and the following relations for the exterior surface are also satisfied;

(19) $$\int (\vec{E}_m \times \vec{H}_n^*) \cdot d\vec{S} = \delta_{mn}$$

(20) $$\int (\vec{E}_{out} \times \vec{H}_m^*) \cdot d\vec{S} = 0$$

(21) $$\int (\vec{E}_m \times \vec{H}_{out}^*) \cdot d\vec{S} = 0$$

From eqs.(17) $-$ (21) coupling coefficient A_m is given by,

(22) $$A_m(z) = \int (\vec{E} \times \vec{H}_m^*) \cdot d\vec{S} = \int (\vec{E}_m \times \vec{H}^*) \cdot d\vec{S}$$

The content of m mode in the receiving waveguide is equal to $|A_m|^2$ because of the orthnormal relationship on EM-field. This formulation can be applied to the off-axis receiving waveguide by shifting the numerical data of $\vec{E}$ and $\vec{H}^*$ in the on-axis receiving waveguide by the amount of the off-axis distance.

The mode analysis in the various receiving-waveguide size (diameter d_r = 95.25, 101.6 and 107.95 mm) is carried out when $TE_{15,2}$ mode at 84 GHz is radiated from the waveguide with d_i = 101.6 mm. Figure 2(a) shows power transmission coefficients for $TE_{15,2}$, and normalized total input-power coefficient P_{in} as a function of z. As shown in Fig. 2(a) for d_r = 101.6 mm, the radiated $TE_{15,2}$ power of 90 % is transmitted at z = 15 mm. In Fig. 2(b), a considerable content (20 %) of mode-converted $TE_{15,3}$ is excited in d_r = 107.95 mm even if high P_{in}. As shown in Fig. 2(c), around 15% of mode $-$ converted $TE_{15,1}$ is excited for d_r = 95.25 mm and main $TE_{15,2}$ mode is as small as 15 %. The optimized d_r, where an amount of sprious mode is as small as posible, is equal to d_i.

For the HE_{11} mode in the corrugated waveguide with $d_i = d_r$ = 88.9 mm, 99.8 % of HE_{11} mode is transmitted at z = 2.5 cm as shown Fig. 3. For reference, the result derived from analytical formula $1.3\sqrt{(\lambda z/2R^2)^3}$ (db) [4] is slightly larger than the numerical calculation.

When the receiving waveguide is in a off-axis position with displacement along $\vec{E}_y$, cross-polarized hybrid mode (XHE_{21}) or its degenerated mode TM_{02} is excited. The calculation for 3 mm displacement of 88.9 mm waveguide at $z = 10$ mm shows 0.5 % of the sprious mode and 98.6 % of HE_{11} mode propagates. The content of sprious mode at $z = 0$ mm is almost the same. For the 45-degrees diplacement to $\vec{E}_y$ the sprious mode of HE_{21} and XHE_{21} modes or TE_{01} and TM_{02} modes which are degenerated are excited. For the displacement of $x = y = 2$ mm, 0.2 % of HE_{21} and XHE_{21} modes or 0.2 % of TE_{01} and TM_{02} modes exists at $z = 10$ mm. Total content of the sprious mode is 0.4 %. These results show that no careful adjustment of the axis is necessary.

§ 4. Phase-Correction Bend

The mode-conversion losses in a 90-degrees HE_{11} bend with flat mirror are calculated by substituting $z = 2\ R$ for the split waveguide. For a bend with $2\ R =$ 88.9 mm, the calculated mode-conversion loss at 84 GHz is 1.2 % ($-$ 19 db) as shown in Fig. 3. The experimental results from normal and cross radiation patterns show that mode-conversion losses for E- and H-bends are $-$ 18 db and $-$ 22db, respectively. The comparison of the experiment with the calculation is in good agreement. The phase correction Φ to make the largest power transfer is obtained by compensating the sum of wave phase at the flat mirror injected from each inlet of the elbow bend ;

$$\Phi(x, y, z) = -\arg[E_y(x, y, R - y)] - \arg[E_y(x, y, R + y)] \tag{23}$$

The calculated contour Φ on the flat mirror for every 10 degrees, and the phase changes along the vertical direction for $x = 0$, 12.7 and 25.4 mm are plotted in Figs. 4(a) and (b). The correction for optimum curved mirror is as small as 38 degrees (0.377 mm) compared with the periphery of the mirror due to the large diameter of corrugated waveguide.

§ 5. Rectangular Corrugated Waveguide

The Gaussian beam with the waist size of x-direction different from that of y-direction is necessary for the limitation in port-size of the vaccum vessel and for the rectangular window in the gyrotron installing internally the Vlasov convertor. The rectangular waveguide with $a \times b$ has two parallel corrugated plates with anisotropic impedance wall and the other two wall being plane metalic. The dispersion relation, EM-fields and attenuation constant are evaluated. In the system, y- and z-

components of the Herz vector are zero and x-component of Herz vector Π_x is given by

$$\Pi_x = \sin(\frac{n\pi x}{a})[\exp(-i\gamma y) \pm \exp(i\gamma(y-b))]\exp(-i\beta z) \tag{24}$$

Here, plus (minus) sign represents symmetric (anti-symmetric) mode and n is the mode number along x-axis. The EM-fields are calculated from

$$\vec{E} = -i\omega\mu_0 \nabla \times \vec{\Pi} \tag{25}$$

$$\vec{H} = k_0^2 \vec{\Pi} + \nabla\nabla \cdot \vec{\Pi}. \tag{26}$$

The dispersion relation is obtained from the equation where the surface impedance of the corrugated plate Z_{cor} is equal to $Z_w = \pm E_y/H_z$ on the surface of $y = b$ and $y = 0$:

$$Z_{cor} = \frac{iWZ_0}{P} \frac{\tan(k_0 d\sqrt{1-(n\lambda/2a)^2})}{\sqrt{1-(n\lambda/2a)^2}} \tag{27}$$

$$Z_w = -\frac{i\gamma Z_0}{k_0} \frac{\tan(\gamma b/2)}{[1-(n\lambda/2a)^2]} \quad \text{for symmetric mode} \tag{28}$$

$$Z_w = \frac{i\gamma Z_0}{k_0} \frac{\cot(\gamma b/2)}{[1-(n\lambda/2a)^2]} \quad \text{for anti} - \text{symmetric mode} \tag{29}$$

where, d, P and W is depth, pitch and width of corrugation. For body mode γ is real and for surface mode γ imaginary. In Figs. 5(a) and (b), $|\beta|$ (rad/cm) and $|\gamma b/\pi|$ as a function of $D(= d/(\lambda/4))$ is shown for $W/P = 0.5$, $n = 1$, $a = b = 1.625$ cm and $\omega/\ 2\ \pi = 84$ GHz. It is shown that γ is equal to $l\pi/b$ (l = odd (even) number for symmetric (anti-symmetric) mode). The attenuation constant α (db/m) calculated by using the perturbation method is also shown in Fig. 5(c). The fields of E_y and H_x components have $\cos(n\pi\xi/a)\cos(l\pi\eta/b)$ when the corrugated depth is $\lambda/\ 4$. Here, the origin of (ξ, η) is in the center of waveguide. For $n = l = 1$ and $a = b$, the function is approximately equal to $J_0(r\chi_{01}/R)$ of HE_{11} mode in the cylindrical corrugated waveguide with the radius of R when $a = R\pi\sqrt{2}/\chi_{01}$. Thus, the conversion from the circular waveguide to rectangular one is easy. The exact calculation of conversion efficiency is now under the way.

§ 6. Rotating-Whispering-Gallery Mode Generator

The rotating-whispering-gallery (RWG) mode with $TE_{15,3}$ is designed and fabricated. The generator is the oversized circular waveguide wound helically by the rectangular waveguide where the only dominant TE_{10} mode propagates. Helical pitch φ_p of rectangular waveguide is detemined by the phase velocity of $TE_{15,3}$ mode at the wall. The wavenumber of RWG mode at the wall is

$$k_r = \sqrt{k_c^2 - k_\theta^2} \tag{30}$$

$$k_\theta = m/R \tag{31}$$

$$k_z = \sqrt{k_0^2 - k_c^2} \tag{32}$$

where $k_c = \chi_{mn}/R$ is the cutoff wavenumber and k_θ the wavenumber of θ-direction. The rotational direction of RWG mode is determined by the sign of k_θ. The angle φ_{gw} between the rectanglar waveguide wound and wavevector $\vec{k}_w$ of RWG mode at the wall is equal to $|\arccos(k_g/k_w)|$. Here, k_g is the wavenumber at the wall of oversized waveguide excited by the curved rectangular waveguide and $|k_w| = \sqrt{k_\theta^2 + k_z^2}$. The angle φ_w of $\vec{k}_w$ with respect to the z-axis is $|\arccos(k_z/k_w)|$. Thus, the pitch angle of the rectagular waveguide φ_p by

$$\varphi_p = \varphi_w \pm \varphi_{gw}. \tag{33}$$

Because another propagating wave for $+z$ direction is also excited in the case of minus sign in eq.(33), we choose φ_p with larger angle than RWG mode. The EM-field emits in the oversized waveguide from the multiholes on the rectangular waveguide through the H-plane coupling (H_z- and H_θ-coupling) or the off-center E-plane coupling (E_r-, H_z- and H_θ-coupling). The calculation shows the total coupling coefficient to the main waveguide is the order of $-$ 40db. As shown in Figs. 6 (a), (b) and (c), contours of Poynting flux $|P|$, radiating angles of Poynting flux $\theta = \arctan(P_y/P_x)$ and $\varphi = \arctan(P_z/\sqrt{P_x^2 + P_y^2})$ at $z = 8$ mm radiated from 84GHz rotating $TE_{15,3}$ mode in the waveguide of 33 mm in diameter are calculated by the SPW method. Rays emitting from the coustic and going to the coustic strongly interference with small flux $|P|$ for $r < R$. In the peak of $|P|$ for $r > R$, the angle φ is as larger as the bounce angle of $TE_{15,3}$ mode in the waveguide, and the angle θ, however, is much smaller than $\arctan(x/y)$ in the waveguide. Experimental radiation pattern with the E-plane coupler shows existence of other higher-mode in addition to rotating $TE_{15,3}$

mode. Low higer-mode can be diminished by inserting the resistive rod in the center of the generator. In the H-plane coupler, low higher-mode almost disappears. The experiment on the connection with the Vlasov anntena is being carried out.

§ 7. Summary

The radiation from the oversized transmission elements for millimeter waves is measured. The experimental results are compared with the calculation based on the superposition of plane wave method and on the Fresnel approximation in the Hugens-Kirchhoff integral. It is confirmed that the fabricated transmission elements have a good peformance. Analysis on split waveguide for whispering gallery mode of $TE_{15,2}$ and hybrid mode of HE_{11} is carried out from the viewpoint of on- and off-axes. The results are useful the split waveguide for gyrotron with radial extracted beam and the dc-cut for waveguide component. By using superposition of plane wave method, the phase correction for a 90-degrees bend is calculated. For large diameter waveguide with HE_{11} mode the correction near the periphery is as small as 40 degrees. We design rotating whispering-gallery-mode generator which is the oversized circular waveguide wound helically by the rectangular waveguide. The calculation on the direction (θ and φ) of Poynting flux of TE15,3 radiated from the circular waveguide shows strong interference with small flux within the diameter of waveguide and θ is much smaller than $\arctan(x/y)$ and φ is as larger as the bounce angle.

ACKNOWLEDMENTS

The authors would like to express appreciation to Drs. A. Iiyoshi and M. Fujiwara for thier continuous encouragement. We thank the members of plasma heating division for thier discussions. This work was supported by a Grant in Aid under the Monbusho Internatonal Scientific Reserch Program (No.03044156).

REFERENCES

[1] Y.T. Lo, S.W. Lee: Antenna Handbook / Theory Applications and Design Van Nostrand Reinhold Company, New York, 1988.

[2] J. Doane: Infrared and Millimeter Waves Vol.13, 123, Academic Press (1985).

[3] Y. Aoki, S. Ishizuka:J. Inst. Electrical Communication of Japan Vol.57-B, 511 (1974) (in Japanese).

[4] W. Henle, A. Jacobs, W. Kasparek, H. Kumrić, G.A. Müller, P.G. Schüller and M. Thumm: EUR-FU / 80 / 90-99, Oct. (1990).

FIGURE CAPTIONS

Fig.1: The experimental and calculated radiation patterns with normal (E_y) and cross (E_x) polarizations for various z. The distance z is 2, 30 and 100 cm for top, middle and bottom patterns, respectively. The calculation is performed for pure HE_{11}-mode. All the contours are plotted by every 2 db for experimental patterns and 5 db for calculated ones. The calculated patterns are normalized by the maximum. Here, P_{cmax}/P_{nmax} which is the ratio of maximum power in cross- to normal-polarization is $-28\pm$ 2db in the experiments and $-$ 45.8 db in the calculation.

Fig.2: (a) Power transmission coefficients for $TE_{15,2}$ mode and suprious-mode contents of $TE_{15,1}$ and $TE_{15,3}$ modes and total input power to the recieving waveguide P_{in} vs. gap distance z. Here, an 84-GHz HE_{11} mode is radiated from the waveguide with 101.6 mm in diameter and is detected with the waveguide of the same diameter.
(b) The calculation condition is the same as that in Fig. 2(a) except the receiving waveguide with 107.95 mm in diameter.
(c) The calculation condition is the same as that in Fig. 2(a) except the receiving waveguide with 95.25 mm in diameter.

Fig.3: (a) Power transmission coefficients for HE_{11} mode and total input power to the recieving waveguide P_{in} vs. gap distance z.
(b) Mode content of HE_{12} and HE_{13} modes vs. gap distance. Here, an 84-GHz HE_{11} mode is radiated from the waveguide with 88.9 mm in diameter and is detected with the receiving waveguide with the same diameter. Analytical result of $1.3\sqrt{(\lambda z/2R^2)^3}$ (db) is also plotted in Fig. 3(a).

Fig.4: (a) Calculated contour of phase with 84-GHz HE_{11} mode on the flat mirror in a 90-degrees bend with 88.9 mm in diameter for every 10 degrees.
(b) Phase variation along $x = 0$, 12.7 and 25.4 mm corresponding to Fig. 4(a).

Fig.5: Characteristics of the rectangular waveguide with two corrugated plates and two plane walls of $a = b = 16.25$ mm , $W/P = 0.5$ and $n = 1$ for $\omega/2\pi = 84$ GHz.
(a) The propagation constant $|\beta|$ (rad/cm) as a function of the normalized corrugated depth D.
(b) Eigen value $|\gamma b/\pi|$ as a function of D.

(c) Attenuation constant α (dB/m) as a function of D.

Fig.6: Charcteristics of radiation at $z = 8$ mm from the rotating 84-GHz $TE_{15,2}$ mode in the waveguide with 33 mm in diameter. Here, the size of screen is 13.2 $\times$ 13.2 cm and the radius of the waveguide is referred to as R.
(a) Contour plots of Poynting flux $|P|$ and profile of $|P|$ along x-axis.
(b) Contour plots of θ =arctan(P_y/P_x) by every 60 degrees.
(c) Contour plots of φ =arctan$(P_z/\sqrt{P_x^2 + P_y^2})$ by every 10 degrees and profile of φ along x-axis.

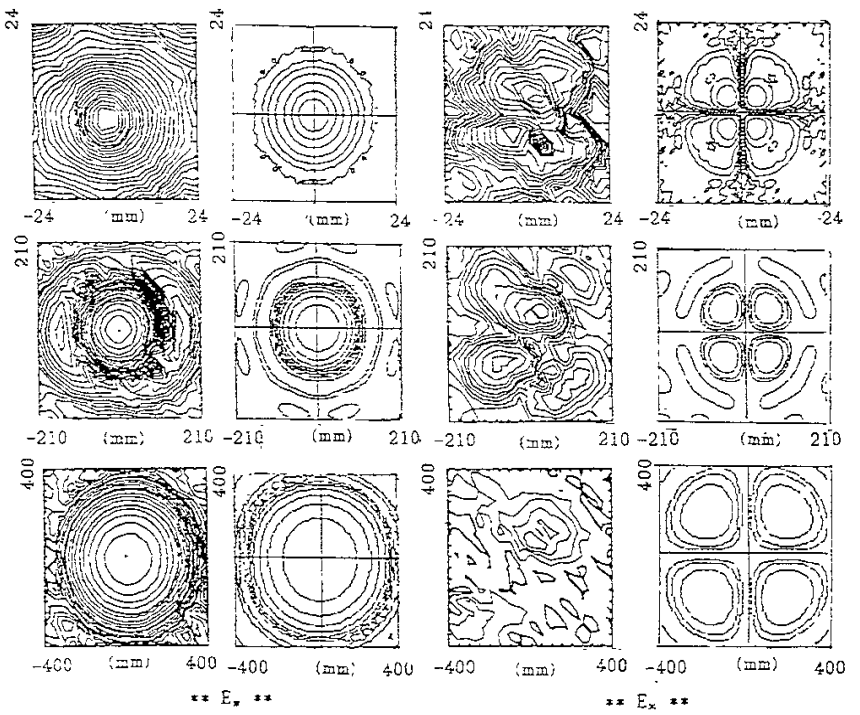
24
-24
(mm)
210
-210
400
-400
** E_y **
** E_x **

Fig. 1

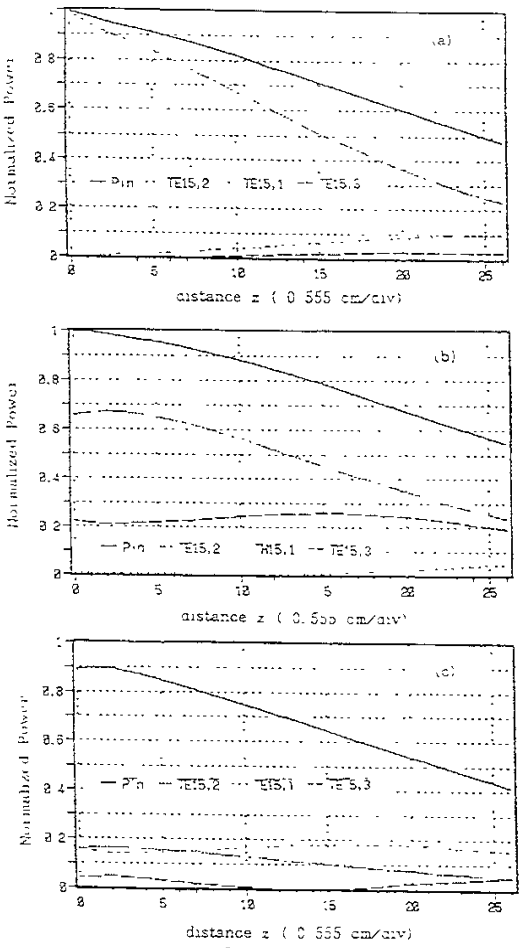
(a)
(b)
(c)
Normalized Power
distance z (0.555 cm/div)

Fig. 2

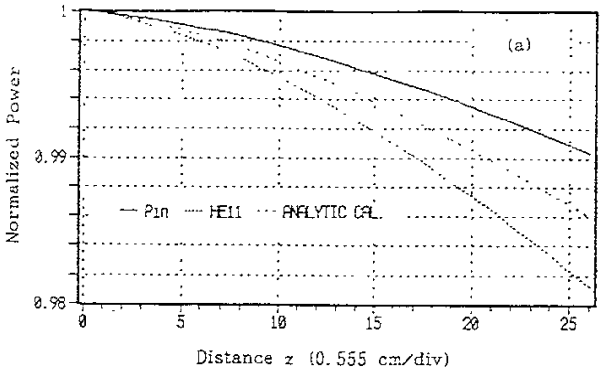
(a)
Normalized Power
1
0.99
0.98
Pin
HE11
ANALYTIC CAL.
0
5
10
15
20
25
Distance z (0.555 cm/div)

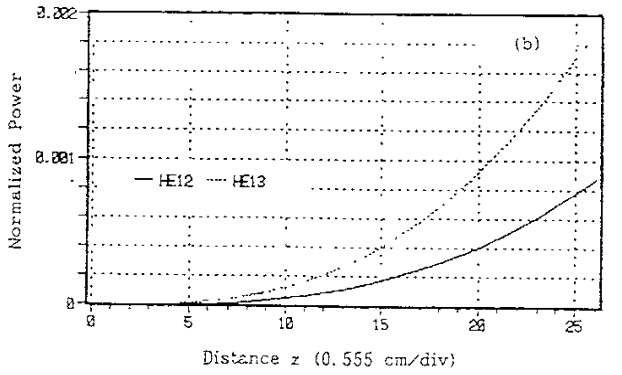
(b)
Normalized Power
0.002
0.001
0
HE12
HE13
0
5
10
15
20
25
Distance z (0.555 cm/div)

Fig. 3

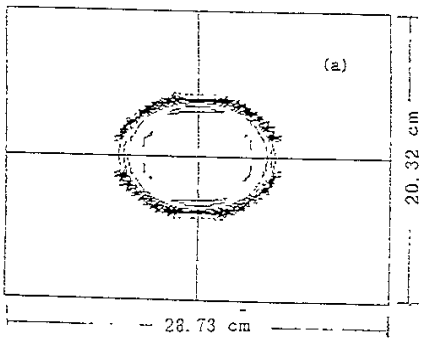
(a)
20.32 cm
28.73 cm

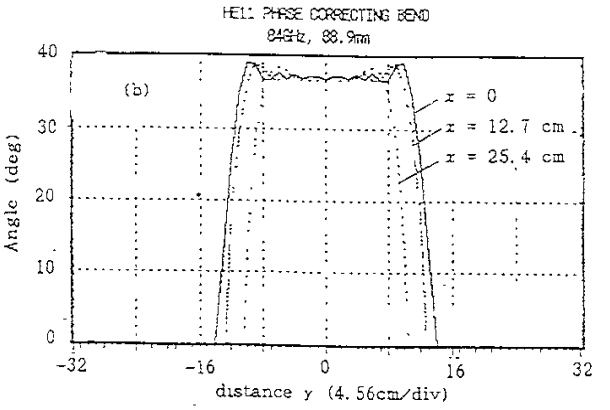
HE11 PHASE CORRECTING BEND
84GHz, 88.9mm
(b)
Angle (deg)
40
30
20
10
0
x = 0
x = 12.7 cm
x = 25.4 cm
-32
-16
0
16
32
distance y (4.56cm/div)

Fig. 4

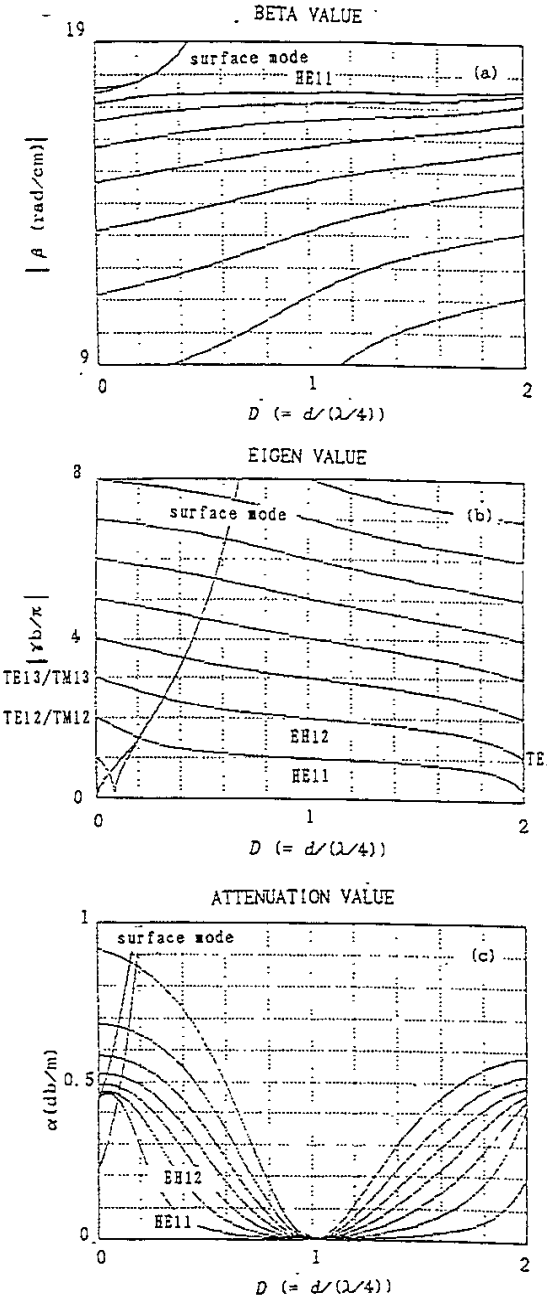
BETA VALUE
19
9
surface mode
HE11
(a)
| β (rad/cm) |
0
1
2
D (= d/(λ/4))
EIGEN VALUE
8
4
0
surface mode
(b)
| γb/π |
TE13/TM13
TE12/TM12
EH12
HE11
TE11/TM11
TE10
0
1
2
D (= d/(λ/4))
ATTENUATION VALUE
1
0.5
0
surface mode
(c)
α (db/m)
EH12
HE11
0
1
2
D (= d/(λ/4))

Fig. 5.

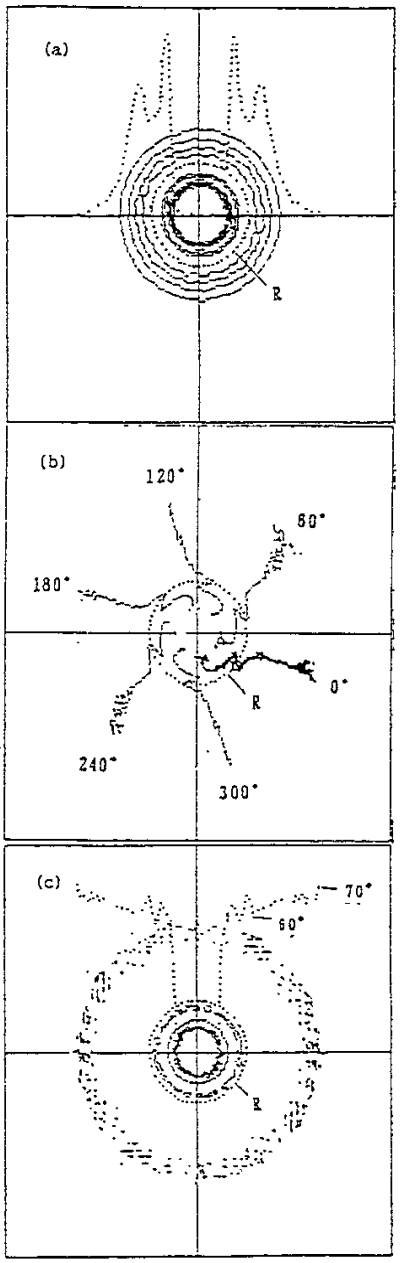
(a)
R
(b)
120°
60°
180°
0°
R
240°
300°
(c)
70°
60°
R

Fig. 6

Recent Issues of NIFS Series

NIFS-166 Vo Hong Anh and Nguyen Tien Dung, *A Synergetic Treatment of the Vortices Behaviour of a Plasma with Viscosity*; Sep. 1992

NIFS-167 K. Watanabe and T. Sato, *A Triggering Mechanism of Fast Crash in Sawtooth Oscillation*; Sep. 1992

NIFS-168 T. Hayashi, T. Sato, W. Lotz, P. Merkel, J. Nührenberg, U. Schwenn and E. Strumberger, *3D MHD Study of Helias and Heliotron;* Sep. 1992

NIFS-169 N. Nakajima, K. Ichiguchi, K. Watanabe, H. Sugama, M. Okamoto, M. Wakatani, Y. Nakamura and C. Z. Cheng, *Neoclassical Current and Related MHD Stability, Gap Modes, and Radial Electric Field Effects in Heliotron and Torsatron Plasmas;* Sep. 1992

NIFS-170 H. Sugama, M. Okamoto and M. Wakatani, *K- ε Model of Anomalous Transport in Resistive Interchange Turbulence* ; Sep, 1992

NIFS-171 H. Sugama, M. Okamoto and M. Wakatani, *Vlasov Equation in the Stochastic Magnetic Field* ; Sep. 1992

NIFS-172 N. Nakajima, M. Okamoto and M. Fujiwara, *Physical Mechanism of E_ϕ-Driven Current in Asymmetric Toroidal Systems* ; Sep.1992

NIFS-173 N. Nakajima, J. Todoroki and M. Okamoto, *On Relation between Hamada and Boozer Magnetic Coordinate System* ; Sep. 1992

NIFS-174 K. Ichiguchi, N. Nakajima, M. Okamoto, Y. Nakamura and M. Wakatani, *Effects of Net Toroidal Current on Mercier Criterion in the Large Helical Device* ; Sep. 1992

NIFS-175 S. -I. Itoh, K. Itoh and A. Fukuyama, *Modelling of ELMs and Dynamic Responses of the H-Mode* ; Sep. 1992

NIFS-176 K. Itoh, S.-I. Itoh, A. Fukuyama, H. Sanuki, K. Ichiguchi and J. Todoroki, *Improved Models of β-Limit, Anomalous Transport and Radial Electric Field with Loss Cone Loss in Heliotron / Torsatron* ; Sep. 1992

NIFS-177 N. Ohyabu, K. Yamazaki, I. Katanuma, H. Ji, T. Watanabe, K. Watanabe, H. Akao, K. Akaishi, T. Ono, H. Kaneko, T. Kawamura, Y. Kubota, N. Noda, A. Sagara, O. Motojima, M. Fujiwara and A. Iiyoshi, *Design Study of LHD Helical Divertor and High Temperature Divertor Plasma Operation* ; Sep. 1992

NIFS-178 H. Sanuki, K. Itoh and S.-I. Itoh, *Selfconsistent Analysis of Radial Electric Field and Fast Ion Losses in CHS Torsatron / Heliotron* ; Sep. 1992

NIFS-179 K. Toi, S. Morita, K. Kawahata, K. Ida, T. Watari, R. Kumazawa, A. Ando, Y. Oka, K. Ohkubo, Y. Hamada, K. Adati, R. Akiyama, S. Hidekuma, S. Hirokura, O. Kaneko, T. Kawamoto, Y. Kawasumi, M. Kojima, T. Kuroda, K. Masai, K. Narihara, Y. Ogawa, S. Okajima, M. Sakamoto, M. Sasao, K. Sato, K. N. Sato, T. Seki, F. Shimpo, S. Tanahashi, Y. Taniguchi, T. Tsuzuki, *New Features of L-H Transition in Limiter H-Modes of JIPP T-IIU* ; Sep. 1992

NIFS-180 H. Momota, Y. Tomita, A. Ishida, Y. Kohzaki, M. Ohnishi, S. Ohi, Y. Nakao and M. Nishikawa, *D-^{3}He Fueled FRC Reactor "Artemis-L"* ; Sep. 1992

NIFS-181 T. Watari, R. Kumazawa, T. Seki, Y. Yasaka, A. Ando, Y. Oka,O. Kaneko, K. Adati, R. Akiyama, Y. Hamada, S. Hidekuma, S. Hirokura, K. Ida, K. Kawahata, T. Kawamoto, Y. Kawasumi, S. Kitagawa, M. Kojima, T. Kuroda, K. Masai, S. Morita, K. Narihara, Y. Ogawa, K. Ohkubo, S. Okajima, T. Ozaki, M. Sakamoto, M. Sasao, K. Sato, K. N. Sato, F.Shimpo, H. Takahashi, S. Tanahasi, Y. Taniguchi, K. Toi, T. Tsuzuki and M. Ono, *The New Features of Ion Bernstein Wave Heating in JIPP T-IIU Tokamak* ;Sep, 1992

NIFS-182 K. Itoh, H. Sanuki and S.-I. Itoh, *Effect of Alpha Particles on Radial Electric Field Structure in Torsatron / Heliotron Reactor*; Sep. 1992

NIFS-183 S. Morimoto, M. Sato, H. Yamada, H. Ji, S. Okamura, S. Kubo, O. Motojima, M. Murakami, T. C. Jernigan, T. S. Bigelow, A. C. England, R. S. Isler, J. F. Lyon, C. H. Ma, D. A. Rasmussen, C. R. Schaich, J. B. Wilgen and J. L. Yarber, *Long Pulse Discharges Sustained by Second Harmonic Electron Cyclotron Heating Using a 35GH$_Z$ Gyrotron in the Advanced Toroidal Facility*; Sep. 1992

NIFS-184 S. Okamura, K. Hanatani, K. Nishimura, R. Akiyama, T. Amano, H. Arimoto, M. Fujiwara, M. Hosokawa, K. Ida, H. Idei, H. Iguchi, O. Kaneko, T. Kawamoto, S. Kubo, R. Kumazawa, K. Matsuoka, S. Morita, O. Motojima, T. Mutoh, N. Nakajima, N. Noda, M. Okamoto, T. Ozaki, A. Sagara, S. Sakakibara, H. Sanuki, T. Seki, T. Shoji, F. Shimbo, C. Takahashi, Y. Takeiri, Y. Takita, K. Toi, K. Tsumori, M. Ueda, T. Watari, H. Yamada and I. Yamada, *Heating Experiments Using Neutral Beams with Variable Injection Angle and ICRF Waves in CHS* ; Sep. 1992

NIFS-185 H. Yamada, S. Morita, K. Ida, S. Okamura, H. Iguchi, S. Sakakibara, K. Nishimura, R. Akiyama, H. Arimoto, M. Fujiwara, K. Hanatani, S. P. Hirshman, K. Ichiguchi, H. Idei, O. Kaneko, T. Kawamoto, S. Kubo, D. K. Lee, K. Matsuoka, O, Motojima, T. Ozaki,

V. D. Pustovitov, A. Sagara, H. Sanuki, T. Shoji, C. Takahashi, Y. Takeiri, Y. Takita, S. Tanahashi, J. Todoroki, K. Toi, K. Tsumori, M. Ueda and I. Yamada, *MHD and Confinement Characteristics in the High-β Regime on the CHS Low-Aspect-Ratio Heliotron / Torsatron* ; Sep. 1992

NIFS-186 S. Morita, H. Yamada, H. Iguchi, K. Adati, R. Akiyama, H. Arimoto, M. Fujiwara, Y. Hamada, K. Ida, H. Idei, O. Kaneko, K. Kawahata, T. Kawamoto, S. Kubo, R. Kumazawa, K. Matsuoka, T. Morisaki, K. Nishimura, S. Okamura, T. Ozaki, T. Seki, M. Sakurai, S, Sakakibara, A. Sagara, C. Takahashi, Y. Takeiri, H. Takenaga, Y. Takita, K. Toi, K. Tsumori, K. Uchino, M. Ueda, T. Watari, I. Yamada, *A Role of Neutral Hydrogen in CHS Plasmas with Reheat and Collapse and Comparison with JIPP T-IIU Tokamak Plasmas* ; Sep. 1992

NIFS-187 K. Ioth, S.-I. Itoh, A. Fukuyama, M. Yagi and M. Azumi, *Model of the L-Mode Confinement in Tokamaks* ; Sep. 1992

NIFS-188 K. Itoh, A. Fukuyama and S.-I. Itoh, *Beta-Limiting Phenomena in High-Aspect-Ratio Toroidal Helical Plasmas*; Oct. 1992

NIFS-189 K. Itoh, S. -I. Itoh and A. Fukuyama, *Cross Field Ion Motion at Sawtooth Crash* ; Oct. 1992

NIFS-190 N. Noda, Y. Kubota, A. Sagara, N. Ohyabu, K. Akaishi, H. Ji, O. Motojima, M. Hashiba, I. Fujita, T. Hino, T. Yamashina, T. Matsuda, T. Sogabe, T. Matsumoto, K. Kuroda, S. Yamazaki, H. Ise, J. Adachi and T. Suzuki, *Design Study on Divertor Plates of Large Helical Device (LHD)* ; Oct. 1992

NIFS-191 Y. Kondoh, Y. Hosaka and K. Ishii, *Kernel Optimum Nearly-Analytical Discretization (KOND) Algorithm Applied to Parabolic and Hyperbolic Equations* : Oct. 1992

NIFS-192 K. Itoh, M. Yagi, S.-I. Itoh, A. Fukuyama and M. Azumi, *L-Mode Confinement Model Based on Transport-MHD Theory in Tokamaks* ; Oct. 1992

NIFS-193 T. Watari, *Review of Japanese Results on Heating and Current Drive* ; Oct. 1992

NIFS-194 Y. Kondoh, *Eigenfunction for Dissipative Dynamics Operator and Attractor of Dissipative Structure* ; Oct. 1992

NIFS-195 T. Watanabe, H. Oya, K. Watanabe and T. Sato, *Comprehensive Simulation Study on Local and Global Development of Auroral Arcs and Field-Aligned Potentials* ; Oct. 1992

NIFS-196 T. Mori, K. Akaishi, Y. Kubota, O. Motojima, M. Mushiaki, Y. Funato and Y. Hanaoka, *Pumping Experiment of Water on B and LaB_6 Films with Electron Beam Evaporator* ; Oct., 1992

NIFS-197 T. Kato and K. Masai, *X-ray Spectra from Hinotori Satellite and Suprathermal Electrons* ; Oct. 1992

NIFS-198 K. Toi, S. Okamura, H. Iguchi, H. Yamada, S. Morita, S. Sakakibara, K. Ida, K. Nishimura, K. Matsuoka, R. Akiyama, H. Arimoto, M. Fujiwara, M. Hosokawa, H. Idei, O. Kaneko, S. Kubo, A. Sagara, C. Takahashi, Y. Takeiri, Y. Takita, K. Tsumori, I. Yamada and H. Zushi, *Formation of H-mode Like Transport Barrier in the CHS Heliotron / Torsatron* ; Oct. 1992

NIFS-199 M. Tanaka, *A Kinetic Simulation of Low-Frequency Electromagnetic Phenomena in Inhomogeneous Plasmas of Three-Dimensions* ; Nov. 1992

NIFS-200 K. Itoh, S.-I. Itoh, H. Sanuki and A. Fukuyama, *Roles of Electric Field on Toroidal Magnetic Confinement,* Nov. 1992

NIFS-201 G. Gnudi and T. Hatori, *Hamiltonian for the Toroidal Helical Magnetic Field Lines in the Vacuum*; Nov. 1992

NIFS-202 K. Itoh, S.-I. Itoh and A. Fukuyama, *Physics of Transport Phenomena in Magnetic Confinement Plasmas*; Dec. 1992

NIFS-203 Y. Hamada, Y. Kawasumi, H. Iguchi, A. Fujisawa, Y. Abe and M. Takahashi, *Mesh Effect in a Parallel Plate Analyzer*; Dec. 1992

NIFS-204 T. Okada and H. Tazawa, *Two-Stream Instability for a Light Ion Beam -Plasma System with External Magnetic Field;* Dec. 1992

NIFS-205 M. Osakabe, S. Itoh, Y. Gotoh, M. Sasao and J. Fujita, *A Compact Neutron Counter Telescope with Thick Radiator (Cotetra) for Fusion Experiment*; Jan. 1993

NIFS-206 T. Yabe and F. Xiao, *Tracking Sharp Interface of Two Fluids by the CIP (Cubic-Interpolated Propagation) Scheme,* Jan. 1993

NIFS-207 A. Kageyama, K. Watanabe and T. Sato, *Simulation Study of MHD Dynamo : Convection in a Rotating Spherical Shell*; Feb. 1993

NIFS-208 M. Okamoto and S. Murakami, *Plasma Heating in Toroidal Systems*; Feb. 1993

NIFS-209 K. Masai, *Density Dependence of Line Intensities and Application to Plasma Diagnostics*; Feb. 1993